

1 Probing conduction band offsets and confined states at GaAs/GaAsN_{Bi} heterointerfaces

2 T.-Y. Huang¹, J. Occena¹, C. Greenhill¹, T. Borrely^{3,4}, Y.-C. Yang¹, J. Hu¹, A. Chen¹, C. Zinn²,
3 K. Jenkins², L. Li^{2,3}, C. Kurdak^{2,3} and R.S. Goldman^{1,2,3*}

⁴ *¹Department of Materials Science and Engineering, University of Michigan,*

5 *²Applied Physics Program, University of Michigan*

6 *³Department of Physics, University of Michigan, Ann Arbor*

7 *Michigan 48109-2136, USA*

8 *⁴Institute of Physics, University of São Paulo*

9 *São Paulo 05508-090, Brazil*

¹⁰*Corresponding author: rsgold@umich.edu

11 **October 08, 2023**

12 ABSTRACT

13 We probe the conduction-band offsets (CBOs) and confined states at GaAs/GaAsNbI
14 quantum wells (QWs). Using a combination of capacitance-voltage (C-V) measurements and self-
15 consistent Schrödinger-Poisson simulations based on the effective mass approximation, we
16 identify a N-fraction dependent increase in CBO, consistent with trends predicted by the band anti-
17 crossing (BAC) model. Using the computed confined electron states in conjunction with
18 photoluminescence spectroscopy (PL) data, we show that N mainly influences the conduction band
19 and confined electron states, with a relatively small effect on the valence band and confined hole
20 states in the quaternary QWs. This work provides important insights toward tailoring CBO and
21 confined electron energies, both needed for optimizing infrared optoelectronic devices.

This is the author's peer reviewed, accepted manuscript. However, the online version of record will be different from this version once it has been copyedited and typeset.

PLEASE CITE THIS ARTICLE AS DOI: 10.1063/5.0172295

22 It has been reported that dilute fractions of N and Bi incorporated into GaAs lead to
23 significant band gap reductions¹⁻⁷ while maintaining lattice-matching with GaAs. In particular, it
24 was recently shown that a N:Bi ratio = 0.83 is needed for lattice matching of the quaternary
25 GaAsNBi to GaAs.⁸ In addition to this material's promise for infrared detectors and laser diodes,⁹⁻
26 ¹⁴ solar cells based upon the quaternary GaAsNBi were recently reported.¹⁵

27 For GaAsNBi, several theoretical models predict that dilute N fractions lower the GaAs
28 conduction band edge (CBE), while dilute Bi fractions raise the GaAs valence band edge (VBE),
29 both on the order of 100 meV for every 1% N or Bi.¹⁶⁻²¹ Thus, co-incorporation of N and Bi is
30 expected to enable independent control of the conduction-band offset (CBO) and valence-band
31 offset (VBO) with respect to GaAs. Beyond computational studies, both C-V measurements and
32 THz spectroscopy have been used to quantify the CBO and VBO of the ternaries. For example,
33 CV measurements of GaAs_{0.97}N_{0.03}/GaAs reveal a CBO of 400 ± 10 meV and a VBO of 11 ± 2
34 meV^{22,23} and electroreflectance measurements of GaAsN thin films and multi-quantum wells
35 (MQWs) reveal a CBO/ ΔE_g of 0.85.²⁴ In addition, THz spectroscopy of GaAs_{1-y}Bi_y/GaAs suggests
36 that CBOs range from 90 to 210 meV and VBOs range from 130 to 530 meV for y_{Bi} from 0.03 to
37 0.117.⁴ To date, measurements of the CBO and VBO for the quaternary GaAs_{1-x}N_xBi_y/GaAs
38 have not been reported.

39 Here, we report on the N-fraction dependence CBOs and confined states at GaAs/GaAs₁₋
40 _xN_x and GaAs/GaAs_{1-x}N_xBi_y single QWs. We use carrier concentration profiles from C-V data
41 and confinement energies from Photoluminescence (PL) spectroscopy, in conjunction with
42 Schrödinger-Poisson simulations of the energy band profiles, to extract the CBOs and confined
43 electron and hole states at the QW interfaces. This work provides important insights into tailoring

This is the author's peer reviewed, accepted manuscript. However, the online version of record will be different from this version once it has been copyedited and typeset.

PLEASE CITE THIS ARTICLE AS DOI: 10.1063/5.0172295

44 the CBO, the VBO, and the confined state energies, all critical parameters for performance of
45 quaternary infrared devices.

46 For this study, we prepared a series of QWs and reference samples by molecular-beam
47 epitaxy. Ternary GaAsN and quaternary GaAsNb_i QW were sandwiched between GaAs:Si layers
48 (300 nm and 690 nm), as shown in Fig. 1. To probe the CBOs and confined state energies, QW
49 thicknesses of 10 nm were targeted to achieve a two-dimensional electron gas (2DEG) with single
50 sub-band occupancy. Confirmation of the 2DEG was achieved via temperature-dependence
51 measurements of capacitance and dissipation, as described in supplemental materials. As shown
52 in the scanning transmission electron microscopy (STEM) image in Fig. 2(a), energy-dispersive
53 X-ray spectroscopy (EDS) in Fig. 2(b) and the cross-sectional TEM image in Fig. 2(c), the 10 nm
54 quaternary QW has a graded lower interface and an abrupt upper interface with maximum $y_{Bi} =$
55 0.018, likely due to Bi surface segregation during epitaxy.²⁵⁻²⁷ The reference samples consisted of
56 GaAs:Si, GaAs_{1-x}N_x and GaAs_{1-x-y}N_xBi_y films. N mole fractions of $x_N = 0.03$ (GaAsN) and $x_N =$
57 0.007, 0.019 and 0.024 (GaAsNb_i) were determined using x-ray rocking curves in conjunction
58 with nuclear reaction analysis as described in Ref.28.

59 Room temperature C-V measurements were conducted using a Keithley 4200
60 semiconductor parameter analyzer with AC voltage = 30 mV, frequency = 1MHz, and DC bias
61 swept from 0.5 to -10 V. For comparison, the measured and computed carrier concentration, \hat{n} , at
62 a depth z from the Schottky contact were calculated using the depletion approximation:

$$63 \quad z = \frac{K_s \varepsilon_0 A}{c} \quad (1)$$

$$64 \quad \hat{n}(z) = - \frac{2}{q K_s \varepsilon_0 A^2 d(1/C^2)/dV} \quad (2)$$

65 where K_s is the GaAs dielectric constant, ε_0 the permittivity of free space, A the contact area, q the
66 elementary charge, and V the DC reverse bias.

This is the author's peer reviewed, accepted manuscript. However, the online version of record will be different from this version once it has been copyedited and typeset.

PLEASE CITE THIS ARTICLE AS DOI: 10.1063/5.0172295

67 For the $\text{GaAs}_{1-x-y}\text{N}_x\text{Bi}_y$ QW, PL spectra were collected at 4.25K using a 532 nm
68 continuous-wave laser with excitation power of 5mW. Subsequently, the Varshni model was used
69 to estimate the PL emission energy at 300K:

70
$$E_g(T) = E_g(0) - \frac{\alpha T^2}{\beta + T} \quad (3)$$

71 where $\alpha = 4.3\text{-}6.8 \times 10^{-4}$ eV/K, $\beta = 119\text{-}378$ K.²⁹

72 Capacitance-voltage profiles for (a) the GaAs:Si reference and (b) the GaAsN QW are
73 presented in Fig. 3. As the bias is swept from 0 to 10V, the capacitance decreases from ~ 0.4 nF
74 to ~ 0.1 nF. For the reference samples, the capacitance decreases monotonically with increasing
75 reverse bias voltage. For reverse biases in the range 3 - 5 V, a platform-like feature, indicated by
76 an upward arrow, is likely due to electron accumulation in the QW.^{30,31} Similar platform-like
77 features are observed in the C-V data shown in Fig. 4 for (a) the GaAs:Si reference sample (b)-(d)
78 the GaAsNBi QWs. The C-V data in Figs. 3 and 4 was converted to electron density vs depth using
79 equation (1) and (2), with an emphasis on the vicinity of the QW, resulting in the plots shown in
80 Fig. 5.

81 To quantify the CBOs, we compare the C-V-determined electron density profiles with
82 those computed using 1D Schrödinger-Poisson simulations in the effective mass approximation
83 using nextnano. To extract the best fit values of the CBO and fixed charges, we performed a
84 sensitivity analysis, as described in the supplemental materials. For GaAsN/GaAs QW, our
85 resulting best fit values are CBO = 360 ± 40 meV and interfacial fixed charge = -6.65×10^{11}
86 $|\text{e}|/\text{cm}^2$, as shown in Fig. 5(a). The CBO value is consistent with 400 ± 10 meV reported for a
87 $\text{GaAs}_{0.97}\text{N}_{0.03}/\text{GaAs}$ QW²³ and 349 meV interpolated from electroreflectance measurements of
88 GaAsN films and QWs.²⁴

This is the author's peer reviewed, accepted manuscript. However, the online version of record will be different from this version once it has been copyedited and typeset.

PLEASE CITE THIS ARTICLE AS DOI: 10.1063/5.0172295

89 For the quaternary QWs with $x_N = 0.7\%$, 1.9% and 2.4% , $y_{Bi} = 1.8\%$, the measured and
90 simulated electron density and conduction band (CB) edge profiles are shown in Figs. 5(b)-(d). In
91 this case, the Bi segregation in the quaternary layers is modeled as step-like CBE profiles, and a
92 similar sensitivity analysis is utilized to determine the best fit values for the CBOs and the fixed
93 charges. The CBO values range from 305 ± 10 meV to 365 ± 30 meV with interfacial fixed
94 charges ranging from -3 to $-5.5 \times 10^{11} |e|/cm^2$. The trend of increasing CBO with x_N value is
95 consistent with predicted trends. However, the specific CBO values exceed those predicted by the
96 band-anticrossing (BAC)^{18,19} and the linear combination of isolated nitrogen resonant states
97 (LCINS) models³². Indeed, the layers likely include N configurations that are not accounted for in
98 the BAC and LCINS models, such as N-As or N-N pairs sitting on an arsenic site, termed “split
99 interstitials”. These split interstitials may contribute to a reduced effective bandgap of GaAsN and
100 GaAs(N)Bi.

101 The 4.25K PL spectra for quaternary QWs are shown in Fig. 6 (a). For all three quaternary
102 QWs, emissions in the range 1.18 to 1.22 eV, labeled “E_o”, are the effective band gaps and
103 attributed to recombination from the confined electron (E¹_e) and hole ground states (E_h). In addition,
104 the higher energy emissions at ~ 1.35 eV, labeled “E₁”, are attributed to recombination from the 1st
105 excited electron (E²_e) and E_h. For the quaternary QW with the lowest x_N, a localized N-related state
106 lies within the band gap, resulting in the ~ 1.06 eV emission labeled “E_N”.³³⁻³⁶ For the quaternary
107 QWs with higher x_N values as the CB edge is lowered, the intensity of emission from the N-
108 localized states is decreased²¹, similar to the Bi-states in valence band.³⁷

109 To determine the positions of the hole ground states, we combine the CBOs and E¹_e from
110 C-V data and nextnano simulations with the Varshni-model estimates of room temperature PL
111 emission energies. The values of E_h are calculated by E_{gGaAs} - E¹_e - E_o, as shown in Fig. 6(b).

This is the author's peer reviewed, accepted manuscript. However, the online version of record will be different from this version once it has been copyedited and typeset.

PLEASE CITE THIS ARTICLE AS DOI: 10.1063/5.0172295

112 Table 1 presents the CBOs, room temperature PL emission energies, the values of E_h , and the
 113 energy difference between electron ground states and 1st excited electron states ($E^{1_e} - E^{2_e}$). The
 114 values of E_h show a relatively weak dependence on N fraction, consistent with earlier reports for
 115 GaAsN QWs, MQWs, and thin films that suggest a relatively small VBO compared to CBO.^{22–}
 116 ^{24,38} Thus, for GaAsNBi, N mainly influences the values of the CB, E^{1_e} , with a relatively small
 117 effect on the values of valence band (VB) and E_h . Finally, $E^{2_e} - E^{1_e}$ is 100–110 meV, comparable
 118 to the value of $E_1 - E_o$ (110–170 meV), suggesting that E_1 is due to the recombination from the 1st
 119 excited electron and the hole ground states.

120

121 **Table 1:** Conduction band offset (ΔE_c), confined electron energy (E^{1_e}), confined hole energy (E_h),
 122 effective bandgap (E_o) and energy of N-related (E_N) with respect to the conduction band edge of
 123 GaAs. $E^{2_e} - E^{1_e}$ is 100–110 meV, comparable to the value of $E_1 - E_o$ (110–170 meV), suggesting that
 124 E_1 is due to recombination from E^{2_e} and E_h . Note that “ E_o Varshni @ RT” and “ E_1 Varshni @ RT”
 125 are Varshni-model estimates of room temperature values of E_o and E_1 .

x_N [NRA]	y_{Bi} [EDS]	ΔE_c (eV) [C-V]	E_N (eV) PL @4.25K	E_o (eV) PL @4.25K	E_o (eV) Varshni @RT	E_1 (eV) PL @4.25K	E_1 (eV) Varshni @RT	E^{1_e} (eV) [nextnano]	E_h (eV)	$E^{2_e} - E^{1_e}$ (eV) [nextnano]
0.7%	1.8%	0.305	1.06	1.22	1.14	1.34	1.25	0.247	0.04	0.1
1.9%	1.8%	0.35	0.98	1.18	1.1	1.36	1.27	0.292	0.03	0.1
2.4%	1.8%	0.365	0.97	1.18	1.1	1.36	1.27	0.303	0.02	0.11

126

127 In summary, we have examined the CBO, VBO, and confined state energies for
 128 GaAsNBi/GaAs. The trend of increasing CBO with x_N value is consistent with predicted trends.
 129 Meanwhile, the N fraction in GaAsNBi has a relatively small effect on the values of the VB and

This is the author's peer reviewed, accepted manuscript. However, the online version of record will be different from this version once it has been copyedited and typeset.

PLEASE CITE THIS ARTICLE AS DOI: 10.1063/5.0172295

130 E_h , consistent with earlier studies of GaAsN. This work provides important insights for tailoring
131 CBOs and confined electron energies for improving infrared optoelectronic device applications.

132

133 **Supplementary materials**

134 Details of epitaxial growth of the samples, quantification of compositions and in-plane strain
135 values as well as the evidence of two-dimensional electron gas (2DEG) formation within the QWs
136 are presented in the supplementary materials. In addition, the key parameters, including electron
137 effective masses, conduction band offsets (CBOs) and interfacial fixed charges, for nextnano
138 simulations and the description of sensitivity analysis for extracting the best fit values and error
139 bars of CBOs are also included.

140 **Acknowledgement**

141 We gratefully acknowledge support from the National Science Foundation (Grant No. DMR
142 1810280). The work at UM Physics was supported by the National Science Foundation under
143 Award No. DMR 2004288 (L.L. capacitance spectroscopy). This study was financed in part by the
144 Coordenação de Aperfeiçoamento de Pessoal de Nível Superior – Brasil (CAPES) – Finance Code
145 001. T.-Y. Huang was supported by the Chia-Lun Lo Fellowship and K. Jenkins was supported by
146 the Rackham Merit Fellowship via the Rackham Graduate School at the University of Michigan.

147

148

149

150

151

152

This is the author's peer reviewed, accepted manuscript. However, the online version of record will be different from this version once it has been copyedited and typeset.

PLEASE CITE THIS ARTICLE AS DOI: 10.1063/5.0172295

153 **Figure captions**

154 **Fig. 1:** Sample structure for GaAsN and GaAsNBi QWs. 10 nm ternary GaAsN and quaternary
155 GaAsNBi QW were sandwiched between GaAs:Si layers (300 nm and 690 nm). Following MBE
156 growth, chrome/gold (200/2000 Å) Schottky contacts were evaporated through a shadow mask
157 with 680 µm diameter circular openings.

158 **Fig. 2:** (a) Scanning transmission electron microscopy (STEM) image, (b) line-cut energy-
159 dispersive X-ray spectroscopy (EDS) data, and (c) cross-sectional transmission electron
160 microscopy image of 10 nm quaternary QW. In (b) and (c), a graded lower interface and an abrupt
161 upper interface are apparent. The black squares in (b) are the EDS data points, showing a maximum
162 $y_{Bi} = 0.018$; the blue dashed line is the boxcar averaging of the EDS data.

163 **Fig. 3:** C-V data for (a) the GaAs:Si reference and (b) the GaAsN QW. In (b), the solid curves
164 correspond to C-V data, while the dashed line corresponds to in nextnano computations, with CBO
165 = 360 meV. For reference sample (a), the capacitance monotonically decreases from ~0.4 to ~0.1
166 nF as the bias voltage sweeps from 0 to 10 V. For GaAsN QW in (b), a platform-like feature,
167 indicated by an upward arrow, is apparent, due to the electron accumulation in the QW regions.

168 **Fig. 4:** C-V data for (a) the GaAs:Si reference and (b)-(d) the GaAsNBi QWs. In (b), (c) and (d)
169 the solid curves correspond to C-V data while the dashed lines correspond to nextnano
170 computations, with CBO = 305, 350 and 365 meV. For the reference sample in (a), the capacitance
171 monotonically decreases from ~0.35 to ~0.1 nF with bias voltage from 0 - 10 V. For the GaAsNBi
172 QWs in (b), (c), and (d), the platform-like features are apparent in voltage ranging from 2 to 4 V.

173 **Fig. 5:** CBE and electron density vs depth profiles for (a) the ternary GaAsN QW and (b)-(d) the
174 quaternary GaAsNBi QWs. The solid curves correspond to the C-V data, while the dashed lines

This is the author's peer reviewed, accepted manuscript. However, the online version of record will be different from this version once it has been copyedited and typeset.

PLEASE CITE THIS ARTICLE AS DOI: 10.1063/5.0172295

175 correspond to nextnano computations using the listed CBO values. In all cases, the electron ground
176 states and 1st excited states in the QWs are indicated by the solid gray and orange lines,
177 respectively. For (b)-(d), the Bi segregation in the quaternary layers are modeled as step-like CBE
178 profiles.

179 **Fig. 6:** (a) 4.25K PL spectra of quaternary GaAsNBi QWs, and (b) band-line-ups for GaAsNBi
180 QWs. In (a), emissions in the range 1.18 to 1.22 eV, labeled “E_o”, are effective band gaps and
181 attributed to recombination from E¹_e and E_h. The higher energy emissions at ~1.35 eV, labeled
182 “E₁”, are attributed to recombination from the E²_e and E_h. For the quaternary QW with the lowest
183 x_N, a localized N-related state lies within the bandgap, resulting in the ~1.08eV emission labeled
184 “E_N”. The energies of E_{gGaAs}, E¹_e, E²_e, E_o, E₁ and E_h are shown in (b). The values of E_h are
185 calculated using E_{gGaAs} – E¹_e – E_o.

186

187

188

189

190

191

192

193

194

195

This is the author's peer reviewed, accepted manuscript. However, the online version of record will be different from this version once it has been copyedited and typeset.

PLEASE CITE THIS ARTICLE AS DOI: 10.1063/5.0172295

196

Figure 1



197

198

199

200

201

202

203

204

205

206

207

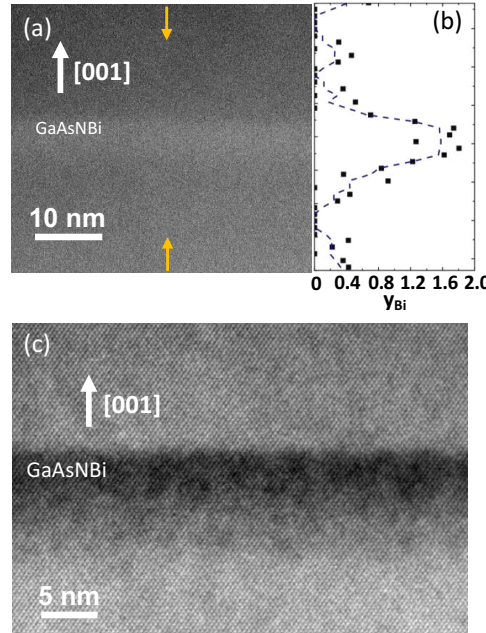
208

209 This is the author's peer reviewed, accepted manuscript. However, the online version of record will be different from this version once it has been copyedited and typeset.

210 PLEASE CITE THIS ARTICLE AS DOI: 10.1063/5.0172295

211
212
213
214
215
216
217
218

Figure 2



This is the author's peer reviewed, accepted manuscript. However, the online version of record will be different from this version once it has been copyedited and typeset.

PLEASE CITE THIS ARTICLE AS DOI: 10.1063/5.0172295

219

220

221

222

223

224

225

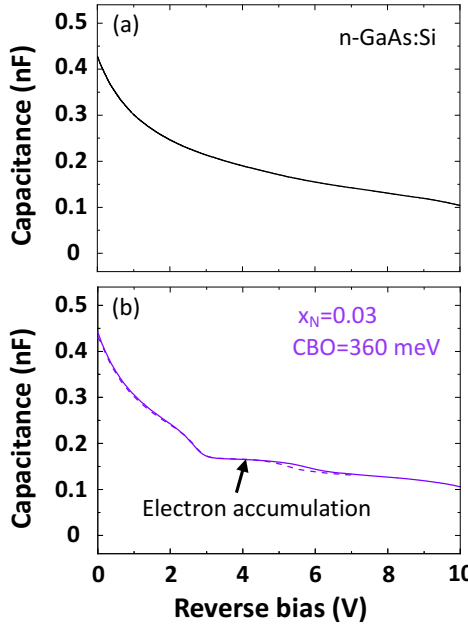
226

227

228

229

Figure 3

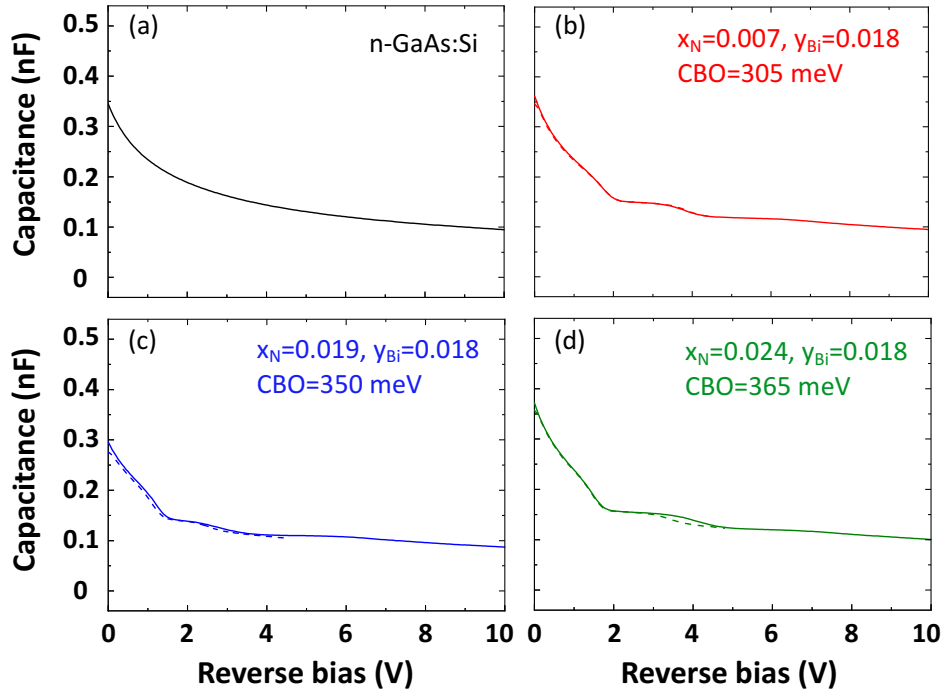


This is the author's peer reviewed, accepted manuscript. However, the online version of record will be different from this version once it has been copyedited and typeset.

PLEASE CITE THIS ARTICLE AS DOI: 10.1063/5.0172295

230

Figure 4



231

232

233

234

235

236

237

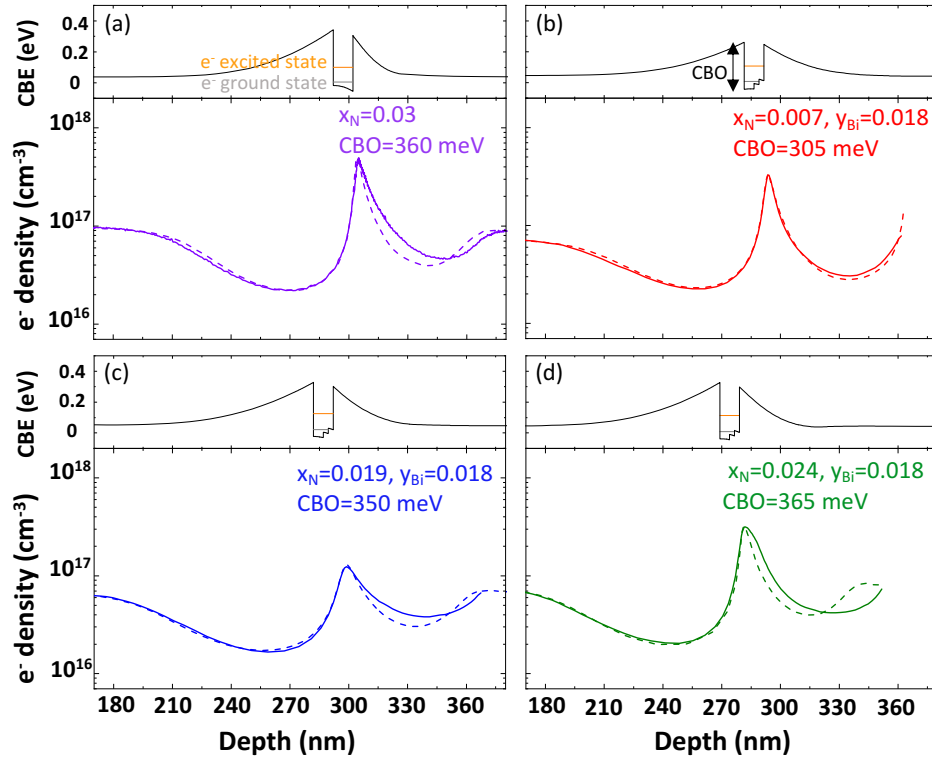
238

This is the author's peer reviewed, accepted manuscript. However, the online version of record will be different from this version once it has been copyedited and typeset.

PLEASE CITE THIS ARTICLE AS DOI: 10.1063/5.0172295

239

Figure 5



240

241

242

243

244

245

246

This is the author's peer reviewed, accepted manuscript. However, the online version of record will be different from this version once it has been copyedited and typeset.

PLEASE CITE THIS ARTICLE AS DOI: 10.1063/5.0172295

247

248

249

250

251

252

253

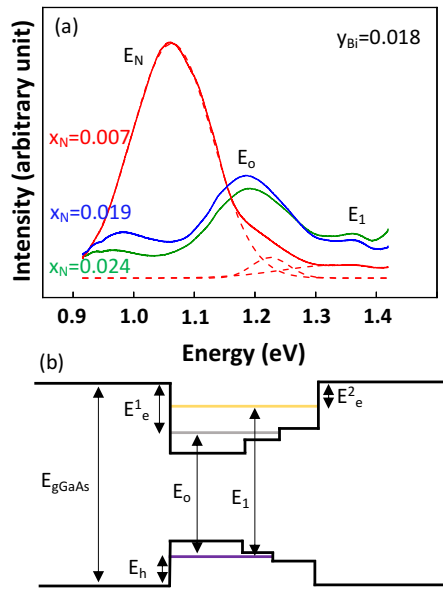
254

255

256

257

Figure 6



This is the author's peer reviewed, accepted manuscript. However, the online version of record will be different from this version once it has been copyedited and typeset.

PLEASE CITE THIS ARTICLE AS DOI: 10.1063/5.0172295

References

- ¹ M. Weyers, M.S.M. Sato, and H.A.H. Ando, "Red Shift of Photoluminescence and Absorption in Dilute GaAsN Alloy Layers," *Jpn. J. Appl. Phys.* **31**, L853 (1992).
- ² S. Francoeur, M.-J. Seong, A. Mascarenhas, S. Tixier, M. Adamcyk, and T. Tiedje, "Band gap of GaAs_{1-x}B_x, 0," *Appl. Phys. Lett.* **82**, 3874.
- ³ K. Uesugi, I. Suemune, T. Hasegawa, T. Akutagawa, and T. Nakamura, "Temperature dependence of band gap energies of GaAsN alloys," *Appl. Phys. Lett.* **76**, 1285 (2000).
- ⁴ V. Karpus, R. Norkus, R. Butkutė, S. Stanionytė, B. Čechavičius, and A. Krotkus, "THz-excitation spectroscopy technique for band-offset determination," *Opt. Express*, **26**, 33807(2018).
- ⁵ P. Klangtakai, S. Sanorpim, K. Yoodee, W. Ono, F. Nakajima, R. Katayama, and K. Onabe, in *2007 2nd IEEE International Conference on Nano/Micro Engineered and Molecular Systems* (2007), pp. 701–706.
- ⁶ Y. Zhang, A. Mascarenhas, H.P. Xin, and C.W. Tu, "Scaling of band-gap reduction in heavily nitrogen doped GaAs," *Phys. Rev. B* **63**, 161303 (2001).
- ⁷ P.H. Tan, X.D. Luo, Z.Y. Xu, Y. Zhang, A. Mascarenhas, H.P. Xin, C.W. Tu, and W.K. Ge, "Photoluminescence from the nitrogen-perturbed above-bandgap states in dilute GaAs_{1-x}N_x alloys: A microphotoluminescence study," *Phys. Rev. B* **73**, 205205 (2006).
- ⁸ J. Occena, T. Jen, J.W. Mitchell, W.M. Linhart, E.-M. Pavelescu, R. Kudrawiec, Y.Q. Wang, and R.S. Goldman, "Mapping the composition-dependence of the energy bandgap of GaAsNBi alloys," *Appl. Phys. Lett.* **115**, 082106 (2019).
- ⁹ M. Yoshimoto, W. Huang, Y. Takehara, K. Oe, A. Chayahara, and Y. Horino, in *16th IPRM. 2004 International Conference on Indium Phosphide and Related Materials, 2004.* (2004), pp. 501–504.
- ¹⁰ M. Yoshimoto, W. Huang, Y. Takehara, J. Saraie, A. Chayahara, Y. Horino, and K. Oe, "New Semiconductor GaNAsBi Alloy Grown by Molecular Beam Epitaxy," *Jpn. J. Appl. Phys.* **43**, L845 (2004).
- ¹¹ W. Huang, M. Yoshimoto, Y. Takehara, J. Saraie, and K. Oe, "GaN_yAs_{1-x-y}B_x Alloy Lattice Matched to GaAs with 1.3 μ m Photoluminescence Emission," *Jpn. J. Appl. Phys.* **43**, L1350 (2004).
- ¹² W. Huang, K. Oe, G. Feng, and M. Yoshimoto, "Molecular-beam epitaxy and characteristics of GaN_yAs_{1-x-y}B_x," *J. Appl. Phys.* **98**, 053505 (2005).
- ¹³ M. Yoshimoto, W. Huang, G. Feng, and K. Oe, "New semiconductor alloy GaNAsBi with temperature-insensitive bandgap," *Phys. Status Solidi (b)* **243**, 1421–1425 (2006).
- ¹⁴ G. Feng, K. Oe, and M. Yoshimoto, "Influence of Thermal Annealing Treatment on the Luminescence Properties of Dilute GaNAs–Bismide Alloy," *Jpn. J. Appl. Phys.* **46**, L764 (2007).
- ¹⁵ H. Kawata, S. Hasegawa, J. Matsumura, H. Nishinaka, and M. Yoshimoto, "Fabrication of a GaAs/GaNAsBi solar cell and its performance improvement by thermal annealing," *Semicond. Sci. Technol.* **36**, 095020 (2021).
- ¹⁶ P.J. Klar, H. Grüning, W. Heimbrodt, J. Koch, W. Stolz, S. Tomić, and E.P. O'Reilly, "Monitoring the non-parabolicity of the conduction band in GaN0.018As0.982/GaAs quantum wells," *Solid-State Electronics* **47**, 437 (2003).
- ¹⁷ P.J. Klar, H. Grüning, W. Heimbrodt, G. Weiser, J. Koch, K. Volz, W. Stolz, S.W. Koch, S. Tomić, S.A. Choulis, T.J.C. Hosea, E.P. O'Reilly, M. Hofmann, J. Hader, and J.V. Moloney,

This is the author's peer reviewed, accepted manuscript. However, the online version of record will be different from this version once it has been copyedited and typeset.

PLEASE CITE THIS ARTICLE AS DOI: 10.1063/5.0172295

"Interband transitions of quantum wells and device structures containing Ga(N, As) and (Ga, In)(N, As)," *Semicond. Sci. Technol.* **17**, 830 (2002).

¹⁸ S.J. Sweeney, and S.R. Jin, "Bismide-nitride alloys: Promising for efficient light emitting devices in the near- and mid-infrared," *J. Appl. Phys.* **113**, 043110 (2013).

¹⁹ N. Ajnef, W.Q. Jemmali, M.M. Habchi, and A. Rebey, "Biaxial strain effects on the band structure and absorption coefficient of $\text{GaAs}_{1-x-y}\text{N}_x\text{Bi}_y/\text{GaAs}$ MQWs calculated using k.p method," *Optik* **223**, 165484 (2020).

²⁰ M. Usman, C.A. Broderick, and E.P. O'Reilly, "Impact of Disorder on the Optoelectronic Properties of $\text{GaN}_y\text{As}_{1-x-y}\text{Bi}_x$ Alloys and Heterostructures," *Phys. Rev. Appl.* **10**, 044024 (2018).

²¹ P.R.C. Kent, and A. Zunger, "Theory of electronic structure evolution in GaAsN and GaPN alloys," *Phys. Rev. B* **64**, 115208 (2001).

²² P. Krispin, S.G. Spruytte, J.S. Harris, and K.H. Ploog, "Electrical depth profile of p-type $\text{GaAs}/\text{Ga(As,N)}/\text{GaAs}$ heterostructures determined by capacitance–voltage measurements," *J Appl. Phys.* **88**, 4153 (2000).

²³ P. Krispin, S.G. Spruytte, J.S. Harris, and K.H. Ploog, "Admittance dispersion of n-type $\text{GaAs}/\text{Ga(As,N)}/\text{GaAs}$ heterostructures grown by molecular beam epitaxy," *J. Appl. Phys.* **90**, 2405 (2001).

²⁴ Y. Zhang, A. Mascarenhas, H.P. Xin, and C.W. Tu, "Formation of an impurity band and its quantum confinement in heavily doped GaAs:N ," *Phys. Rev. B* **61**, 7479 (2000).

²⁵ X. Lu, D.A. Beaton, R.B. Lewis, T. Tiedje, and M.B. Whitwick, "Effect of molecular beam epitaxy growth conditions on the Bi content of $\text{GaAs}_{1-x}\text{Bi}_x$," *Appl. Phys. Lett.* **92**, 192110 (2008).

²⁶ R.B. Lewis, M. Masnadi-Shirazi, and T. Tiedje, "Growth of high Bi concentration $\text{GaAs}_{1-x}\text{Bi}_x$ by molecular beam epitaxy," *Appl. Phys. Lett.* **101**, 082112 (2012).

²⁷ D.A. Beaton, A. Mascarenhas, and K. Alberi, "Insight into the epitaxial growth of high optical quality $\text{GaAs}_{1-x}\text{Bi}_x$," *J. Appl. Phys.* **118**, 235701 (2015).

²⁸ J. Occena, T. Jen, E.E. Rizzi, T.M. Johnson, J. Horwath, Y.Q. Wang, and R.S. Goldman, "Bi-enhanced N incorporation in GaAsNbI alloys," *Appl. Phys. Lett.* **110**, 242102 (2017).

²⁹ W. Żuraw, W.M. Linhart, J. Occena, T. Jen, J.W. Mitchell, R.S. Goldman, and R. Kudrawiec, "Temperature-dependent study of $\text{GaAs}_{1-x-y}\text{N}_x\text{Bi}_y$ alloys for band-gap engineering: photoreflectance and k · p modeling," *Appl. Phys. Express* **13**, 091005 (2020).

³⁰ C.R. Moon, B.-D. Choe, S.D. Kwon, H.K. Shin, and H. Lim, "Electron distribution and capacitance–voltage characteristics of n-doped quantum wells," *J. Appl. Phys.* **84**, 2673 (1998).

³¹ B.M. Tschirner, F. Morier-Genoud, D. Martin, and F.K. Reinhart, "Capacitance-voltage profiling of quantum well structures," *J. Appl. Phys.* **79**, 7005 (1996).

³² E.P. O'Reilly, A. Lindsay, and S. Fahy, "Theory of the electronic structure of dilute nitride alloys: beyond the band-anti-crossing model," *J. Phys.: Condens. Matter* **16**, S3257 (2004).

³³ J.F. Chen, C.T. Ke, P.C. Hsieh, C.H. Chiang, W.I. Lee, and S.C. Lee, "Deep-level emissions in GaAsN/GaAs structures grown by metal organic chemical vapor deposition," *J. Appl. Phys.* **101**, 123515 (2007).

³⁴ D. Sentosa, T. Xiaohong, and C.S. Jin, "Luminescence from the deep level N–N interstitials in GaAsN grown by metal organic chemical vapour deposition," *CrystEngComm* **12**(7), 2153–2156 (2010).

³⁵ M.-C. Hsieh, J.-F. Wang, Y.-S. Wang, C.-H. Yang, C.-H. Chiang, and J.-F. Chen, "Electron Emission Properties of GaAsN/GaAs Quantum Well Containing N-Related Localized States: The Influence of Illuminance," *Jpn. J. Appl. Phys.* **51**, 02BJ12 (2012).

This is the author's peer reviewed, accepted manuscript. However, the online version of record will be different from this version once it has been copyedited and typeset.

PLEASE CITE THIS ARTICLE AS DOI: 10.1063/5.0172295

³⁶ F. Hassen, Z. Zaaboub, M. Bouhlel, M. Naffouti, H. Maaref, and N.M. Garni, "Optical characterization and carriers transfer between localized and delocalized states in Si-doped GaAsN/GaAs epilayer," *Thin Solid Films* **594**, 168 (2015).

³⁷ O. Donmez, A. Erol, M.C. Arikhan, H. Makhlofi, A. Arnoult, and C. Fontaine, "Optical properties of GaBiAs single quantum well structures grown by MBE," *Semicond. Sci. Technol.* **30**, 094016 (2015).

³⁸ R. Kudrawiec, M. Motyka, M. Gladysiewicz, J. Misiewicz, J.A. Gupta, and G.C. Aers, "Contactless electroreflectance of $Ga_{N_y}As_{1-y}/GaAs$ multi quantum wells: The conduction band offset and electron effective mass issues," *Solid State Commun.* **138**, 365 (2006).